Science Press

ARTICLE

Formation Process of CoCrFeNi High Entropy Alloy via Electro-Deoxidization of Metal Oxides in Molten Salt

Yang Yu[1,2], Luo Xiangyu[1,2], Ma Tongxiang[1,2], Hu Liwen[1,2], Wen Liangying[1,2], Hu Meilong[1,2]

[1] College of Materials Science and Engineering, Chongqing University, Chongqing 400044, China; [2] Chongqing Key Laboratory of Vanadium-Titanium Metallurgy and New Materials, Chongqing University, Chongqing 400044, China

Abstract: CoCrFeNi high entropy alloys (HEAs) were prepared by electro-deoxidization of metal oxides in $CaCl_2$ molten salt at 1173 K. The phase transformation from the metal oxides to HEA under different electrolysis durations was investigated by X-ray diffraction (XRD), scanning electron microscopy (SEM), and energy dispersive X-ray spectroscopy (EDS). The results show that the formation process of CoCrFeNi HEA includes two stages: the rapid deoxidization stage and deep deoxidization stage. In the rapid deoxidization stage, 93.93wt% oxygen in sintered oxide pellet is removed within 1 h and the current efficiency reaches 89.95%. After electrolysis of 15 h, the oxygen content of the product is 0.26wt% and the current efficiency is 17.93%. The formation process of CoCrFeNi HEA provides guidance for establishing the electrochemical route with low cost and high efficiency.

Key words: high-entropy alloys; electro-deoxidization; formation process; oxygen content; current efficiency

Generally, the traditional alloys consist of one or two main elements as the matrix and several minor alloying elements for modifying the microstructure and properties[1]. However, the high entropy alloy (HEA), a relatively new type of metallic materials, has attracted much attention for its unique composition, microstructure, and excellent performance. According to the definition proposed by Yeh et al[2], HEAs are typically composed of five or more principal elements in equimolar or near-equimolar ratios, and each principal element concentration is between 5at% and 35at%. Because the large configurational entropy is in favor of the thermo-dynamic stability in equimolar or near-equimolar ratios, the HEAs tend to have a simple solid solution of single-phase structure, and exhibit outstanding properties, such as high strength and hardness, good structure stability, excellent corrosion and oxidation resistance.

At present, the traditional preparation methods of HEAs based on the product state in the preparation process are the liquid method, the solid method, and the gas method[3,4]. But the disadvantages, such as high preparation temperature, high cost, and long process flow, of these preparation methods have restricted the further application of HEAs. The method of the electro-deoxidization in molten salt has demonstrated that HEAs can be synthesized directly from their mixed solid oxides[5]. Compared with the traditional methods, electro-chemical reduction process has the advantages of low temperature and one-step reduction. Currently, many resear-ches about the electro-deoxidization mechanism have been made for different pure metal oxides[6-8]. Sri et al[9] investigated the reaction process during electro-deoxidization of the solid Nb_2O_5 discs in molten $CaCl_2$. The results show that the reaction pathway of Nb_2O_5 is $Ca_xNb_yO_z \rightarrow NbO_2 + NbO \rightarrow Nb$. Jackson et al[10] reported that NiTi alloy prepared via electrochemical reduction in molten $CaCl_2$ involves a series of partial reductions. Firstly, Ni and $CaTiO_3$ are formed rapidly from $NiTiO_3$ precursor. Then, the intermediate compounds Ni_3Ti and Ni-Ti-O appear. Finally, NiTi alloy forms. In addition, the reduction of other pure metal oxides and mixed metal oxides to the pure metals and alloys via electro-deoxidization in molten salt was also investigated. However, the research on the formation process of HEAs has rarely been reported[11].

In this research, the formation process of CoCrFeNi HEA was investigated by varying the electrolysis duration. The

oxygen content and the current efficiency of the specimens after different electro-deoxidization durations were obtained, which provides the guidance for one-step and high efficiency process of HEAs preparation.

1 Experiment

The solid oxide powders (commercially available solid oxide in molar ratio of $CoO:Cr_2O_3:Fe_2O_3:NiO=2:1:1:2$) were mixed in the ball mill for 1 h to ensure the uniformity. In order to keep the similar electro-reduction rate for specimens with different electro-deoxidization durations, NH_4HCO_3 (reagent grade, Sinopharma Chemical Reagent Co., Ltd, Beijing, China) was used as fugitive agent[12]. The homogenized mixed solid oxide powders of 2 g and NH_4HCO_3 of 1 g were placed in a cylindrical mold of 20 mm in diameter and die-pressed at 6 MPa (disc of 3.5 mm in thickness). Then, the die-pressed specimens were dried at 353 K for 1 h to remove the NH_4HCO_3. Finally, the green pellets were sintered at 1173 K for 3 h.

The anhydrous $CaCl_2$ of 500 g (reagent grade, Sinopharma Chemical Reagent Co., Ltd, Beijing, China) was dried at 443 K for 24 h to remove moisture. The reactor was vacuumed and then flowed by argon to remove oxygen. Subsequently, the temperature of the melt in alumina crucible was increased to 1173 K under argon atmosphere to melt salt. Fig. 1 presents the schematic diagram of the experiment platform, electrolysis cell, and appearance of the anode and cathode. The stainless-steel wire mesh (75 μm) and the wire (0.1 mm in diameter) were wrapped around the cathode pellet. The graphite rod (10 mm in diameter and 100 mm in height) was used as the anode. The electrolytic voltage in the experiment was 3.0 V. The electrolysis time ranged from 5 min to 15 h. After electrolysis, the products were ground into powders and washed in deionized water. Finally, the specimens were vacuum-dried at 333 K.

The theoretical decomposition potentials of each oxide into the pure metal at 1173 K were calculated by HSC Chemistry 6.0 software[13], as listed in Table 1. The electrolytic voltage was supplied by DC power supply (DP310, MESTEK, China). The open porosity of the specimens was measured by Archimedes' method. The precursors and the products were characterized by X-ray diffraction (XRD, D/max 2500PC,
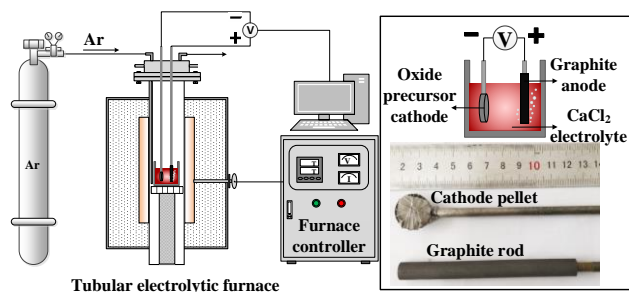
Table 1   Possible reactions and related theoretical decomposition potentials

No.	Reaction	$\Delta G_{1173\,K}$/kJ·mol^{-1}	$E_{1173\,K}$/V
1	$2CoO=2Co+O_2(g)$	303.036	−0.79
2	$Cr_2O_3=2Cr+1.5O_2(g)$	827.988	−1.43
3	$Fe_2O_3=2Fe+1.5O_2(g)$	516.287	−0.89
4	$2NiO=2Ni+O_2(g)$	267.152	−0.69
5	$CaCl_2=Ca+Cl_2(g)$	623.491	−3.23

Rigaku, Japan), scanning electron microscopy (SEM) with backscattered electron (BSE) mode, and energy dispersive X-ray spectroscopy (EDS, TESCAN VEGA II with Oxford INCA Energy 350). The ONH analyzer (THC600, Germany) was used to measure the oxygen content of the cathodic products.

2 Results and Discussion

2.1 Characterization of solid oxide precursors

Fig.2 shows XRD patterns of the mixed oxide powders and the sintered pellet, indicating that no chemical reaction happens during ball milling. The phases of the sintered pellet include $CoCr_2O_4$, $NiCo_2O_4$, $NiCr_2O_4$, and $NiFe_2O_4$, suggesting that the separated oxides can be converted to complex oxides by sintering at 1173 K. This conclusion was also proposed by Sure[14]. In addition, because NH_4HCO_3 escaped when the die-pressed specimens were dried at 353 K for 1 h, the mixed oxide powder is not reduced by NH_4HCO_3.

SEM/EDS analysis was used to verify the homogeneity of the individual oxide particles of precursors, as shown in Fig.3. The obvious sintering phenomenon among the separated original oxides occurs and the pores are distributed in the sintered pellet uniformly, which is caused by the evaporation of NH_4HCO_3 fugitive agent during the sintering process[12]. The open porosity of the specimens prepared under the same condition is 48.37vol%, which provides the same ion diffusion rate in the mixed oxide pellets under different experiment conditions. Fig. 3c presents SEM-BSE image of the sintered

Fig.1   Schematic diagram of experiment platform, electrolysis cell, and appearance of anode and cathode
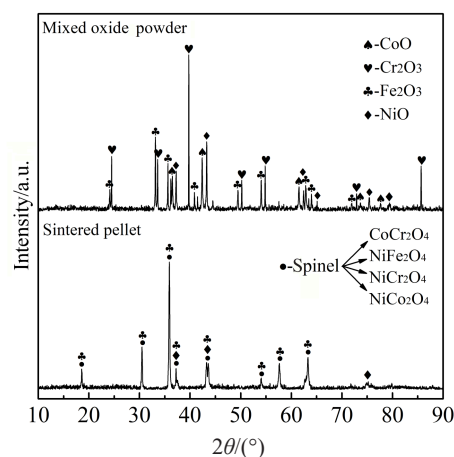

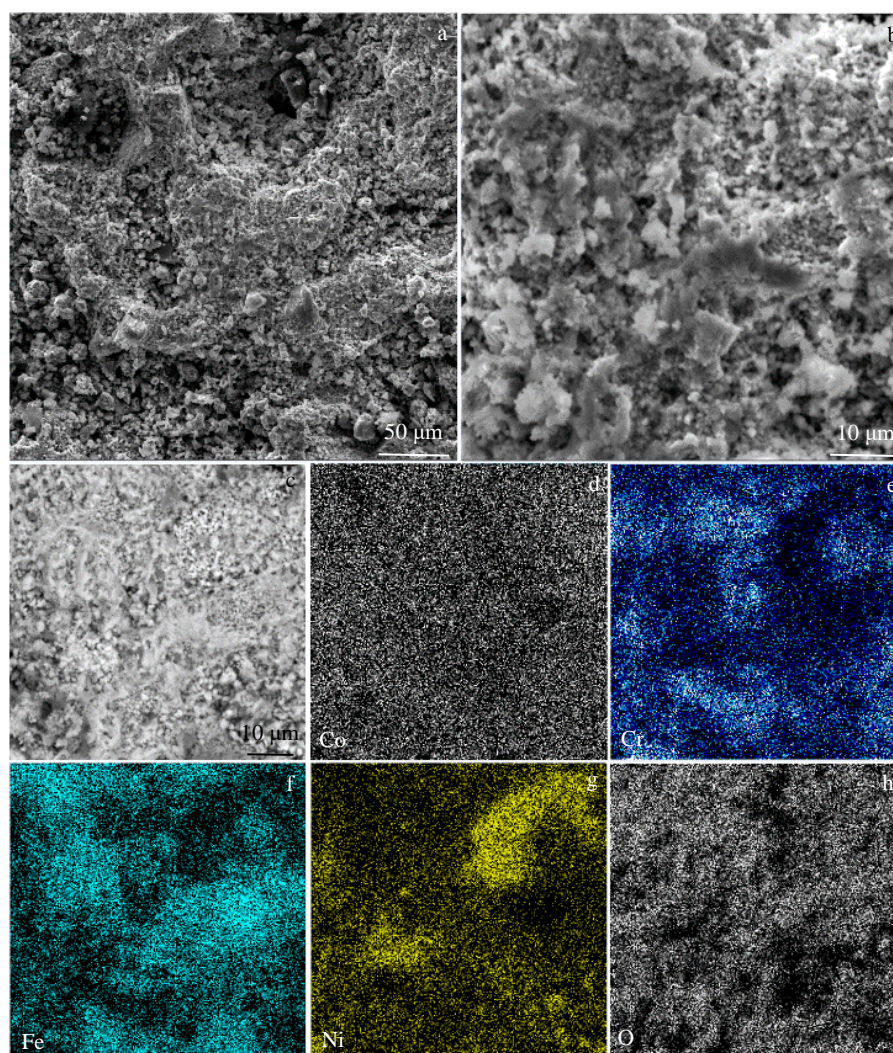Fig.2   XRD patterns of mixed oxide powder and sintered pellet

Fig.3　SEM-BSE images (a~c) and EDS element distributions of Co (d), Cr (e), Fe (f), Ni (g), and O (h) for sintered oxide pellet

pellet. The EDS element distributions reveal that Co is distributed uniformly, Ni is aggregated in a small area, and Fe and Cr are dispersed uniformly in the area without Ni aggregation. XRD results of the sintered pellet show that not all the original oxides are converted into complex oxides in the sintering process. There is some remaining NiO, which leads to the aggregation of Ni. The uniform distribution of Fe and Cr in the area without Ni aggregation is due to the formation of spinel of $CoCr_2O_4$ and Fe_2O_3.

2.2 Electro-deoxidization of solid oxide precursors

The theoretical decomposition voltages of CoO, Cr_2O_3, Fe_2O_3, and NiO at 1173 K are 0.79, 1.43, 0.89, and 0.69 V, respectively. Meanwhile, the generation of CO at anode offers depolarization effect in the electrolytic cell, which promotes the decrease of potential gain[15]. The theoretical decomposition voltage of $CaCl_2$ electrolyte is 3.23 V, indicating that the experiment voltage of 3.0 V in the two-electrode system is insufficient to decompose the $CaCl_2$ electrolyte but sufficient to electro-deoxidize the metal oxides.

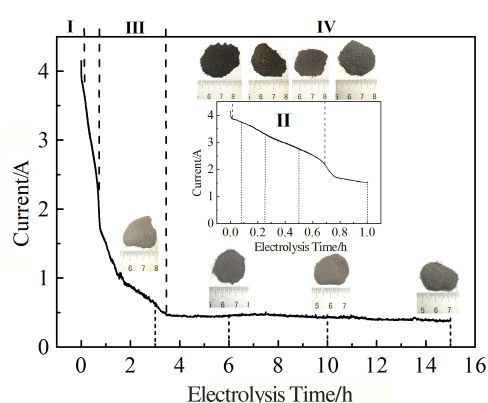Fig.4 presents the current (*I*)-electrolysis time (*t*) curve of

Fig.4　Current (*I*)-electrolysis time (*t*) curve of sintered pellet (inset images are appearance of the products after electrolysis for different time)

the sintered pellet electrolyzed for 15 h. The inset images show that the product powders changed from black to gray with the increase of electrolysis time. There are 4 typical

stages in the *I-t* plot of electro-deoxidization for 15 h in the molten $CaCl_2$ at 1173 K. Firstly, a peak current forms at the beginning of the electrolysis. Then the current decreases sharply from 4.15 A to 3.90 A in a short time. Secondly, the current gradually decreases from 3.90 A to 2.35 A during the following 0.66 h. Thirdly, the current enters a slow decrease stage from 1.77 A to 0.47 A during 0.75~3.5 h after a current quick drop. Finally, the current decreases to a plateau stage, which is close to the background current. The peak current formed at the beginning of the electrolysis mainly benefits from the large reaction area because the cathode pellet surface is covered by stainless steel wire mesh. Different electrolysis durations (5 min, 15 min, 0.5, 1, 3, 6, and 10 h) were selected to investigate the electro-deoxidization and alloy formation process. The inset curve shows the *I-t* curve of electrolysis in 1 h.

2.3 Structure and morphology characterization of cathodic products

XRD patterns were used to identify the composition of the product powders from black to gray, as shown in Fig. 5. According to the changes in diffraction peaks of specimens after different electrolysis durations CoCrFeNi HEA can be found at electrolysis time of 3 h. After electrolysis of 3 h, the phases do not change with further extending the electrolysis time. XRD pattern of product after electrolysis of 5 min shows that the Ni, Co, and $CaCr_2O_4$ appear. On the one hand, the formation of Ni and Co in the first 5 min benefits from the large contact area between cathode oxide pellet and stainless-steel wire mesh due to the large initial reaction interface and good conductivity. On the other hand, the low theoretical decomposition potentials and oxide valence make NiO and CoO easy to be electro-reduced into pure metal. $CaCr_2O_4$ in

the reduced specimens is generated, and calcium ions play an active role in the reduction process and are temporarily found in the cathode[15,16]. Eq. (1) and Eq. (2) reveal the reactions as follows:

$$4Cr_2O_3 + 3Ca^{2+} + 6e^- = 2Cr + 3CaCr_2O_4 \tag{1}$$

$$CaCr_2O_4 + 6e^- = 2Cr + 4O^{2-} + Ca^{2+} \tag{2}$$
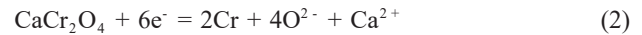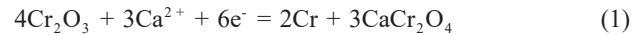
Cr diffraction peak cannot be found in XRD patterns due to the trace content of Cr. Fig. 6 shows the SEM-secondary electron (SE) and SEM-BSE images of the product after electrolysis of 5 min. It can be observed that a small number of other phases (light color phase) are distributed in the specimens. SEM-SE and SEM-BSE images show that the particles precipitated from the matrix in other phases are about 3 μm in size. EDS spectrum of point 1 indicate that the precipitated particles are the alloy phase consisting of Ni, Co, and a little Cr. The EDS spectra of point 2 and 3 indicate that the matrix phase consists of complex oxides and $CaCr_2O_4$.

XRD pattern of specimen after electrolysis for 15 min shows that CoCrFeNi HEA, Fe_2O_3, FeO, and Fe form in this stage. The appearance of CoCrFeNi HEA with face-centered cubic (fcc) structure in specimen is ascribed to the presence of Fe. The calcium ferrite does not form in the electro-reduction process of Fe_2O_3. The reduction of solid Fe_2O_3 is carried out by a two-step reduction: $Fe_2O_3{\rightarrow}FeO{\rightarrow}Fe$. This result agrees with the conclusion of Gao[17].

Hence, the metal of Fe is electrolyzed later than Ni, Co, and Cr. When Fe metal is produced in the molten $CaCl_2$ at 1173 K, the HEA is likely to form among the metal of Ni, Co, Cr, and Fe due to the high entropy effect[18,19]. Fig. 7 shows SEM-BSE images and related EDS spectra of the specimen after electrolysis for 15 min. From the SE images in Fig. 7, the dendritic structure (Fig. 7a and 7d) and the precipitated particles (Fig. 7g) can be observed. EDS analyses were used to identify the special phases in the product. The results of point 1 and 3 indicate that the dendritic structure is composed of Fe, and different morphologies in dendritic structure may be caused by Cr and Co. The results of point 2 and 4 indicate that the matrix phase is mainly composed of $CaCr_2O_4$ and complex oxides. The results of point 5 and 6 represent the phase of Ni and CoCrFeNi HEA, and the morphology of CoCrFeNi HEA is nodular structure, as identified by XRD results.

XRD pattern of specimen after electrolysis for 0.5 h indicates that the spinel phase in the sintered pellet disappears after electrolysis for 0.5 h. The main oxide phases in the cathode product are $CaCr_2O_4$ and Cr_3O, because the theoretical decomposition potential of Cr_2O_3 is higher than that of other metal oxides, which leads to a slow electro-deoxidization process. Besides the main phases of CoCrFeNi HEA, Fe also exists in the cathode product because the dendritic iron does not form CoCrFeNi HEA due to the long diffusion distance with other elements. Fig. 8 shows SEM-SE and SEM-BSE images and EDS spectra of the product after electro-deoxidization for 0.5 h. As shown in Fig. 8b, it can be observed that the main phase has nodular structure. EDS analyses of point 2 and 4 indicate that the nodular structure
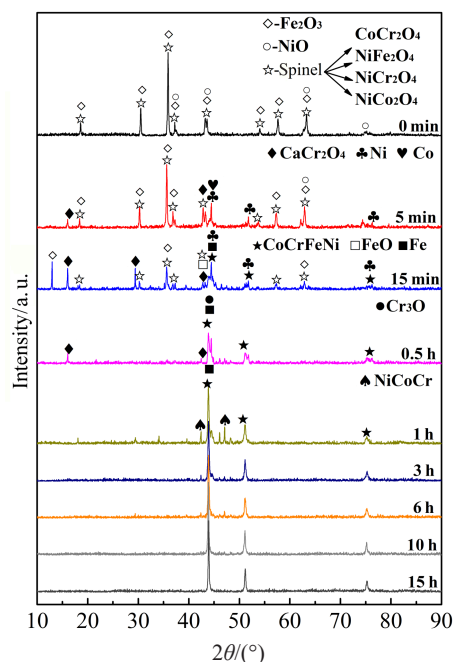
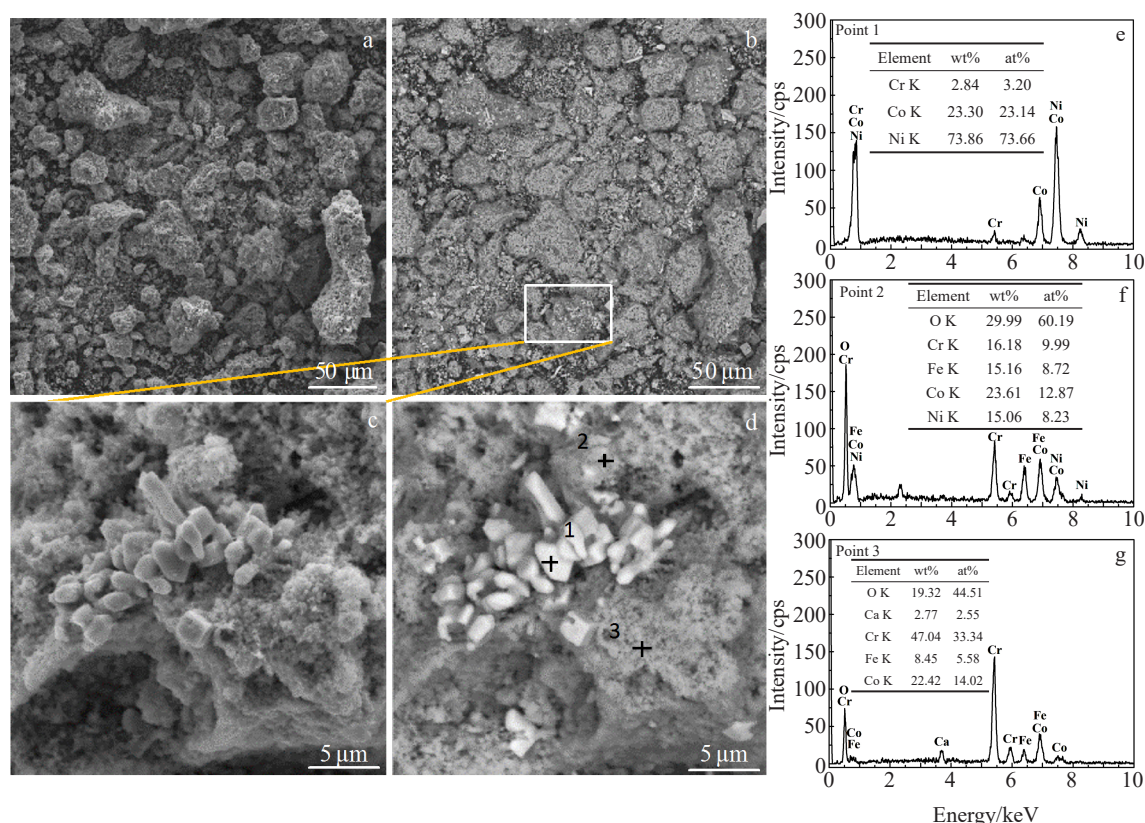Fig.5 XRD patterns of specimens after different electrolysis durations

Fig.6   SEM-SE (a, c) and SEM-BSE (b, d) images of specimen after electrolysis for 5 min; EDS annlysis results of point 1 (e), 2 (f), and 3 (g) in Fig.6d

phase is CoCrFeNi HEA in non-equimolar ratio. EDS analyses of point 1 and 3 exhibit the unreduced $CaCr_2O_4$ and Fe metal, respectively, which do not form HEA.

The cathode product after electrolysis for 1 h consists of CoCrFeNi HEA, metal Fe, and NiCoCr phases. The oxide phases disappear after electrolysis for 1 h in $CaCl_2$ molten salt at 1173 K. Fig. 9 shows the SEM-SE and SEM-BSE images and EDS spectra of the product after electrolysis for 1 h. Fig. 9a and 9d show that the phase of dendritic structure and coupling shape exists in the nodular structure matrix phase. Fig.9b, 9c, 9e, and 9f present the phases of dendritic structure and coupling shape. EDS analyses of point 1 and 2 indicate that the phase of dendritic structure and the coupling shape is Fe-rich phase, which is similar to the phases observed in Fig. 7a and 7b. This result indicates that Fe is reduced and aggregated firstly, and then diffused and alloyed with other elements during the formation process of HEA in molten salt electrolysis.

XRD pattern of the product after electrolysis for 3 h shows that the CoCrFeNi HEA is the only phase in the product. Fig. 10a~10h show SEM-BSE images of the products after electrolysis for 3~15 h. All images reveal a nodular structure with the individual particles closely joined together at their interfaces, and the morphology of CoCrFeNi HEA is not affected by the processing time. Fig.10i~10l display element distributions of the CoCrFeNi HEAs reduced for different durations. The composition of different CoCrFeNi HEAs is listed in Table 2. The result indicates that Fe, Co, and Ni are uniformly distributed and only a small amount of Cr is aggregated in the certain areas. The similar element distributions were also reported by other studies[20,21]. Dai[22] pointed out that the compounds of Cr_7C_3 and $Cr_{23}C_3$ are formed during the electro-deoxidization process, and C element is produced by the side reactions of soluble CO_3^{2-} and calcium ions.

2.4 Oxygen content, current efficiency, and energy consumption of HEAs

There are 4 typical stages of CoCrFeNi HEA formation in the I-t plot. In the second stage, the current gradually decreases from 3.90 A to 2.35 A as electrolysis time ranges from 5 min to 0.5 h. XRD patterns of the specimens after electrolysis for 5 min~0.5 h show that metal oxide phases always exist. However, metal oxide phases disappear in the specimen electrolyzed for 1 h after the current drops. As shown in Fig. 11, it can be concluded that the second stage is the rapid deoxidization stage, in which 93.93wt% oxygen in sintered oxide pellet was removed within 1 h and the current efficiency reaches 89.95%. The decrease of oxygen content of the products after electrolysis for 1~15 h is only 3.11wt% (the oxygen content of specimens after electrolysis for 15 h is 0.26wt%), but the current efficiency decreases from 89.95% to 17.93%. It can be demonstrated that the third and fourth
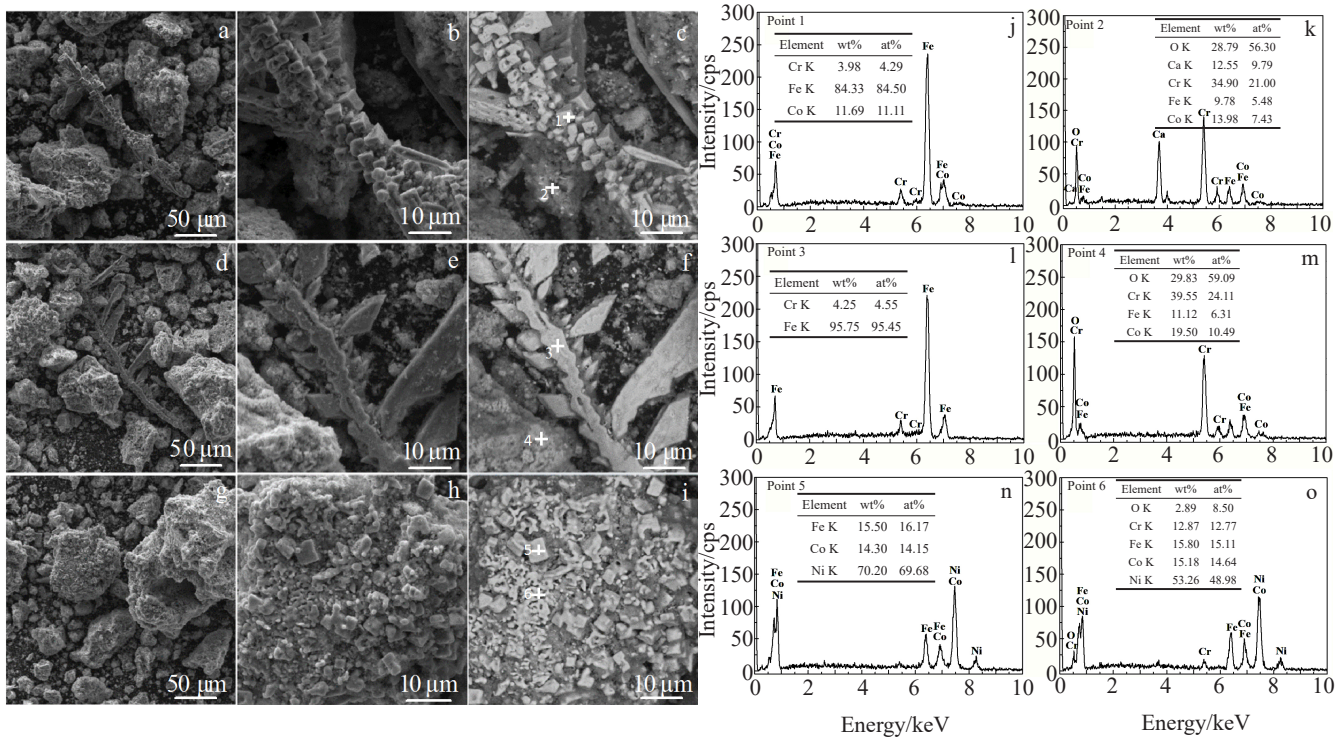
Fig.7   SEM-SE (a, b, d, e, g, h) and SEM-BSE (c, f, i) images of specimen after electrolysis for 15 min; EDS analysis results of point 1 (j), 2 (k) in Fig.7c, point 3 (l), 4 (m) in Fig.7f, and point 5 (n), 6 (o) in Fig.7i
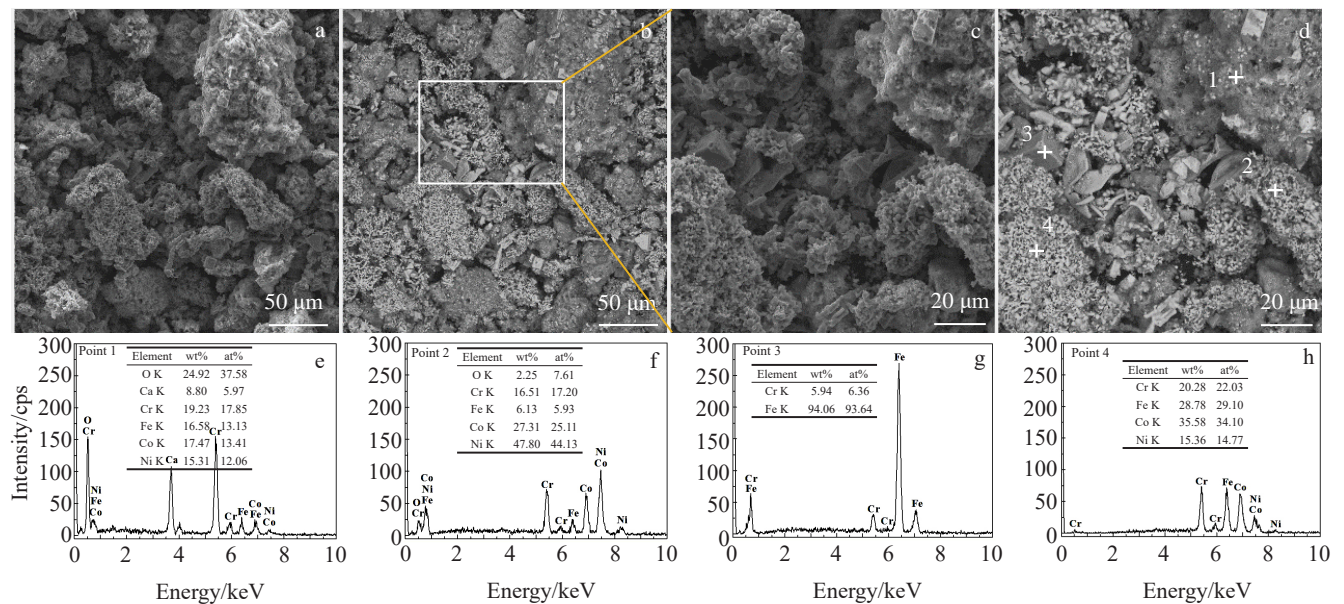

Fig.8   SEM-SE (a, c) and SEM-BSE (b, d) images of specimen after electrolysis for 0.5 h; EDS analysis results of point 1 (e), 2 (f), 3 (g), and 4 (h) in Fig.8d

stages in *I-t* plot is the deep deoxidization stage. The main reason for the low current efficiency is the high background current caused by the side reactions of soluble CO_3^{2-} and calcium ions[23]. In general, the side reactions can be inhibited effectively and the current efficiency is improved significantly by an inert anode[24,25].

The energy consumption of CoCrFeNi HEA preparation

with different oxygen contents is also plotted in Fig. 11. The results show that the energy consumption of specimen after electrolysis of 1 h (3.37wt% oxygen) is 4 kW·h/kg, which is significantly lower than that treated by iron metallurgy. However, the energy consumption increases linearly as oxygen content decreases, and eventually reaches 14.7 kW·h/kg with 0.26wt% oxygen, which is higher than that treated by
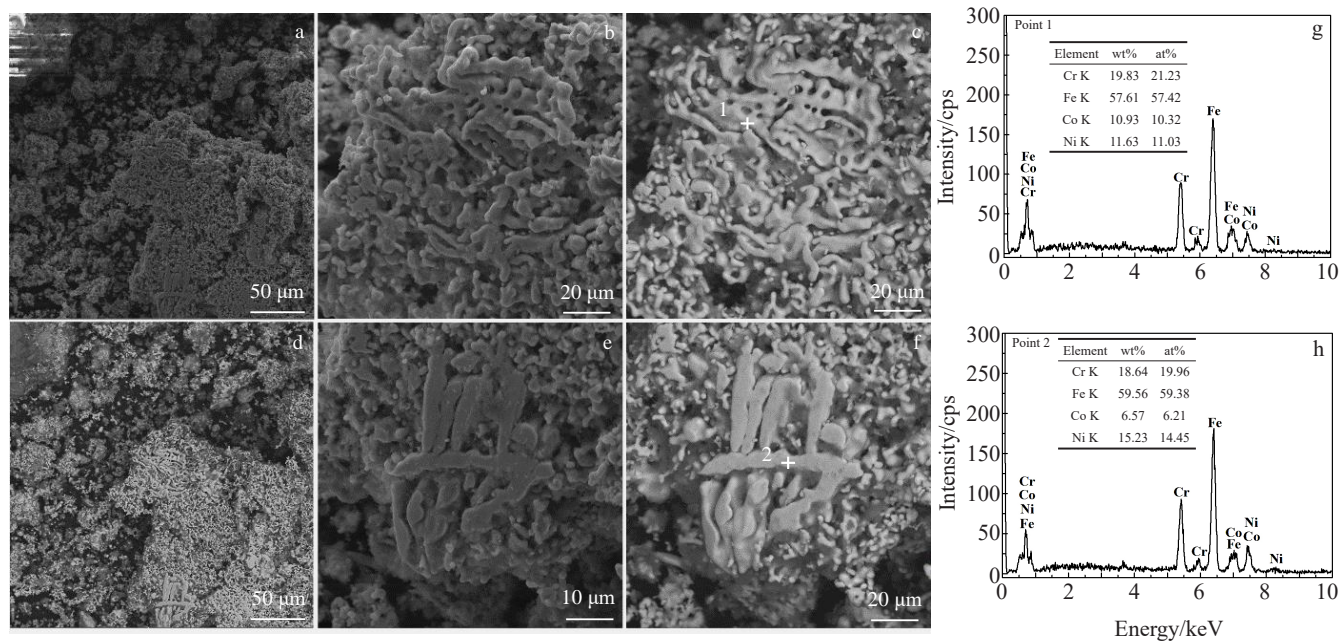
Fig.9　SEM-SE (a, b, d, e) and SEM-BSE (c, f) images of specimen after electrolysis for 1 h; EDS analysis results of point 1 in Fig.9c (g) and point 2 in Fig. 9f (h)
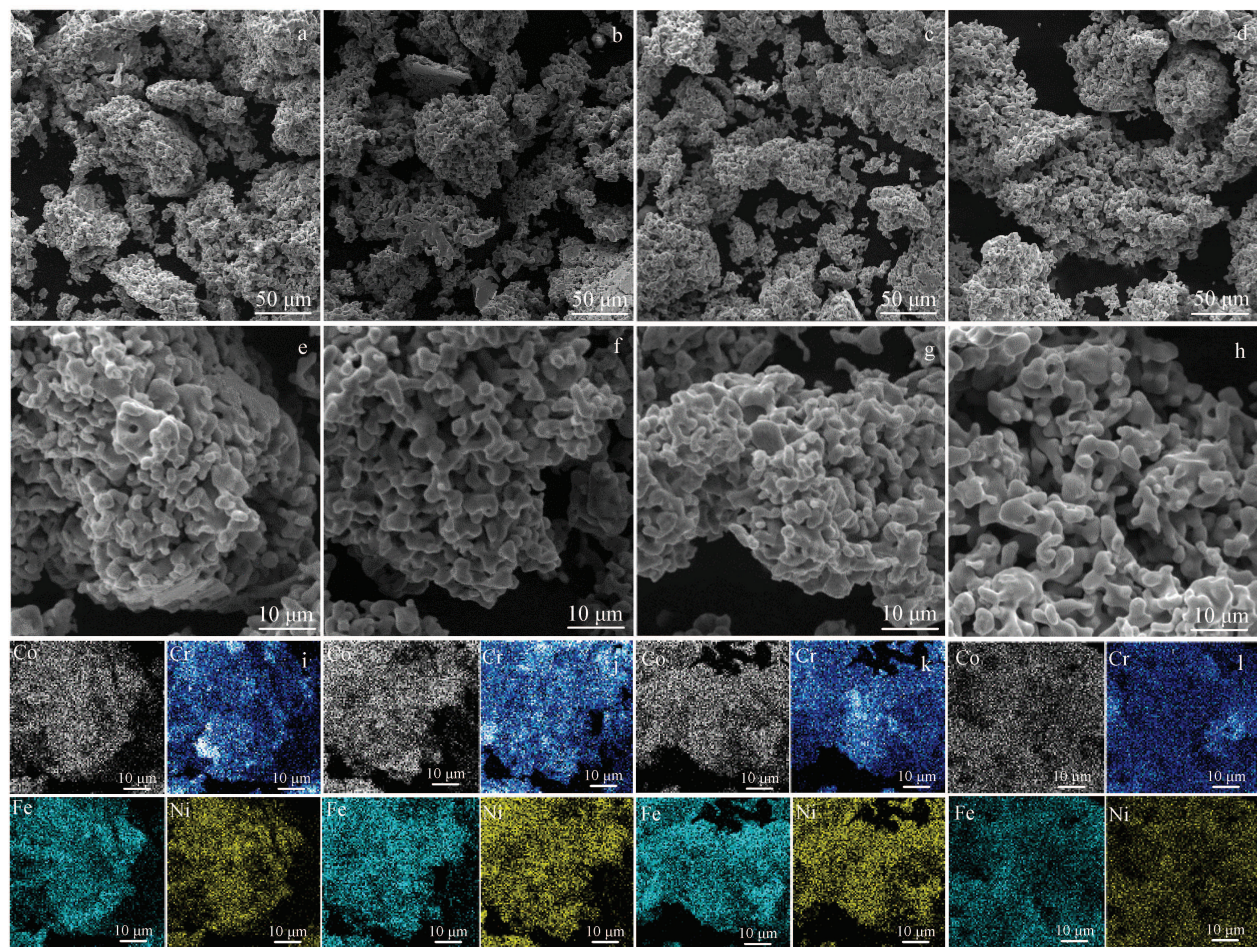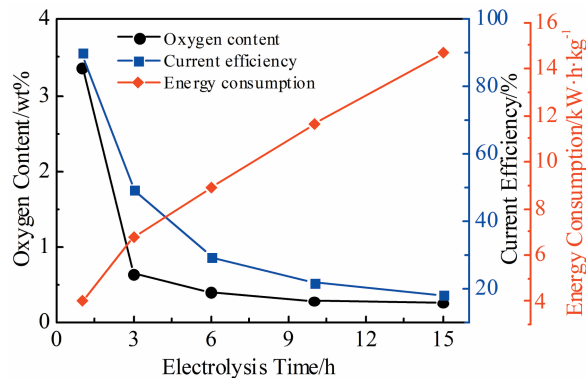

Fig.10　SEM-BSE images (a~h) and corresponding element distributions (i~l) in Fig.10e~10h of specimen after electrolysis for 3 h (a, e, i), 6 h (b, f, j), 10 h (c, g, k), and 15 h (d, h, l)

Table 2 Chemical composition of CoCrFeNi HEAs after different electrolysis durations (at%)

Electrolysis time/h	Cr	Fe	Co	Ni
3	26.81	25.14	25.25	22.80
6	32.34	19.61	27.45	20.60
10	27.20	30.08	23.85	18.87
15	26.54	23.98	27.54	21.94

Fig.11 Oxygen content, current efficiency, and energy consumption curves of specimens after electrolysis for 1~15 h

iron metallurgy. It has been reported that oxygen and carbon doping in HEAs can significantly enhance the strength and ductility[26,27]. In addition, a mixture of the individual metal oxides and graphite was deoxidized in a melt of $CaCl_2$ at 1173 K to synthesize nanoscale (TiNbTaZrHf)C HEA using modern additive manufacturing techniques, and the preliminary tests also indicate a possible application in supercapacitors[28]. The oxygen and carbon doping in HEAs not only solves the problems of cathode carbon pollution and deep deoxidization, but also improves the current efficiency significantly. This result verifies the feasibility of HEAs preparation at low processing temperature, which is a low-energy and high efficiency process.

3 Conclusions

1) The formation process of CoCrFeNi high entropy alloy (HEA) in molten salt during electro-deoxidization of metal oxides consists of two stages: the rapid deoxidization stage and the deep deoxidization stage. In the first stage, 93.93wt% oxygen in sintered oxide pellet is removed within 1 h and the current efficiency reaches 89.95%. In the second stage, the oxygen content of the products after electrolysis for 15 h is 0.26wt%, but the current efficiency is only 17.93%.

2) In the electro-deoxidization process, NiO and CoO are reduced into pure metal more easily than Cr_2O_3 and Fe_2O_3. Fe is reduced and aggregated firstly, and then diffused and alloyed with other elements to form HEA during electrochemical deoxidization. Because the mechanical properties of HEAs can be enhanced by oxygen and carbon doping, the disadvantages of electrochemical reduction with graphite,

such as carbon pollution of cathode, difficulty of deep deoxidization, and low current efficiency, can be conquered.

References

1 Sure J, Vishnu D S M, Schwandt C. *Applied Materials Today*[J], 2017, 9: 111

2 Yeh J W, Chen S K, Lin S J *et al*. *Advanced Engineering Materials*[J], 2004, 6(5): 299

3 Zhang Yong, Zuo Tingting, Tang Zhi *et al*. *Progress in Materials Science*[J], 2014, 61: 1

4 Zhang W R, Liaw P K, Zhang Y. *Science China Materials*[J], 2018, 61(1): 2

5 Chen G Z, Fray D J, Farthing T W. *Nature*[J], 2000, 407(6802): 361

6 Chen G Z, Gordo E, Fray D J. *Metallurgical and Materials Transactions B*[J], 2004, 35(2): 223

7 Qiu Guohong, Ma Meng, Wang Dihua *et al*. *Journal of the Electrochemical Society*[J], 2005, 152(10): 328

8 Abdelkader A M, Kilby K T, Cox A *et al*. *Chemical Reviews*[J], 2013, 113(5): 2863

9 Sri M V D, Sanil N, Shakila L. *Electrochimica Acta*[J], 2013, 100: 51

10 Jackson B, Jackson M, Dye D *et al*. *Journal of the Electrochemical Society*[J], 2008, 155(12): 171

11 Yang Y, Ma T X, Hu M J *et al*. *TMS 2020 149th Annual Meeting & Exhibition Supplemental Proceedings*[C]. San Diego: Springer, 2020: 1593

12 Li Wei, Jin Xianbo, Huang Fulong *et al*. *Angewandte Chemie International Edition*[J], 2010, 49(18): 3203

13 Suzuki R O, Ono K, Teranuma K. *Metallurgical and Materials Transactions B*[J], 2003, 34(3): 287

14 Sure J, Vishnu D S M, Schwandt C. *Journal of Alloys and Compounds*[J], 2019, 776: 133

15 Schwandt C, Fray D J. *Zeitschrift für Naturforschung A*[J], 2007, 62(10-11): 655

16 Hyslop D J S, Abdelkader A M, Cox A *et al*. *Acta Materialia*[J], 2010, 58(8): 3124

17 Gao Haiping, Jin Xianbo, Zou Siwei *et al*. *Electrochimica Acta* [J], 2013, 107: 261

18 Yeh J W. *Annales de Chimie, Science des Materiaux* (*Paris*)[J], 2006, 31(6): 633

19 Yeh J W. *JOM*[J], 2013, 65(12): 1759

20 Maiti S, Steurer W. *Acta Materialia*[J], 2016, 106: 87

21 Wang Bin, Huang Jian, Fan Jinhang *et al*. *Journal of the Electrochemical Society*[J], 2017, 164(14): 575

22 Dai Lei, Lu Yuan, Wang Xianyu *et al*. *International Journal of Refractory Metals and Hard Materials*[J], 2015, 51: 153

23 Jiao H D, Wang M Y, Tu J *et al*. *Journal of the Electrochemical Society*[J], 2018, 165(11): 574

24 Jiao S Q, Fray D J. *Metallurgical and Materials Transactions B* [J], 2010, 41(1): 74

25 Hu L, Song Y, Ge J *et al. Journal of the Electrochemical Society* [J], 2016, 163(3): 33

26 Lei Zhifeng, Liu Xiongjun, Wu Yuan *et al. Nature*[J], 2018, 563(7732): 546

27 Wang Z, Baker I, Cai Z *et al. Acta Materialia*[J], 2016, 120: 228

28 Sure J, Vishnu D S M, Kim H K *et al. Angewandte Chemie International Edition*[J], 2020, 59(29): 11 830

CoCrFeNi高熵合金在金属氧化物熔盐电脱氧中的形成过程

杨　宇[1,2]，罗翔宇[1,2]，马通祥[1,2]，胡丽文[1,2]，温良英[1,2]，扈玫珑[1,2]

(1. 重庆大学 材料科学与工程学院，重庆 400044)

(2. 重庆大学 钒钛冶金与新材料重庆市重点实验室，重庆 400044)

摘　要：在1173 K下将金属氧化物在$CaCl_2$熔盐中进行电脱氧，制备了CoCrFeNi高熵合金。通过X射线衍射（XRD）、扫描电子显微镜（SEM）和能量色散X射线能谱（EDS）研究了不同电解时间下金属氧化物转化为高熵合金的相变过程。结果表明，CoCrFeNi高熵合金的形成过程包括快速脱氧和深度脱氧2个阶段。在快速脱氧阶段，在1 h内去除了烧结氧化物球团中93.93%（质量分数）的氧，电流效率达到89.95%。电解结束后，产物的氧含量可达0.26%（质量分数），电流效率为17.93%。该高熵合金的形成过程可用于指导建立低成本、高效率的电化学路线。

关键词：高熵合金；电脱氧；形成过程；氧含量；电流效率